PERGAMON

International Journal of Heat and Mass Transfer 44 (2001) 2163–2175

International Journal of HEAT and MASS TRANSFER

www.elsevier.com/locate/ijhmt

On the design of two-dimensional cellular metals for combined heat dissipation and structural load capacity

S. Gu [a], T.J. Lu [a,b,*], A.G. Evans [b]

[a] *Department of Engineering, University of Cambridge, Trumpington Street, Cambridge CB2 1PZ, UK*
[b] *Materials Institute, Princeton University, Princeton, NJ 08450, USA*

Received 15 May 2000

Abstract

Sandwich panels with two-dimensional metal cores can be used to carry structural load as well as dissipate heat through solid conduction and forced convection. This work attempts to uncover the nature of heat transfer in these lightweight systems, with emphasis on the effects of varying cell morphologies and cell arrangements. The types of cell shape and cell arrangement considered include regular hexagon, square with connectivity 4 or 3, and triangle with connectivity 6 or 4. Two analytical models are developed: corrugated wall and effective medium. The former models the cellular structure in detail whilst, the latter models the fluid saturated porous structure using volume averaging techniques. The overall heat transfer coefficient and pressure drop are obtained as functions of relative density, cell shape, cell arrangement, fluid properties, and overall dimensions of the heat sink. A two-stage optimization is subsequently carried out to identify cell morphologies that optimize the structural and heat transfer performance at specified pumping power and at lowest weight. In the first stage, the overall heat transfer performance is optimized against relative density. Regular hexagonal cells are found to provide the highest levels of heat dissipation. In the second stage, a constraint on stiffness is added. It is then found that, for panels with thin cores, triangular cells constitute the most compact and yet stiff heat sink design; however, for high heat flux scenarios, hexagonal cells outperform triangular and square cells.

1. Introduction

For decades there has been considerable interest in cellular solids made of an interconnected network of solid struts or plates which form the edges and faces of cells [1–3]. The simplest is a two-dimensional array of polygons which pack to fill a plane area. Regular hexagonal honeycombs are used as cores of sandwich panels in engineering structures where high stiffness/strength at minimum weight is essential. Recent advances in low-costing processes have enabled micro-cell to be used as compact heat exchangers where high surface area density is required [4,5]. An intriguing situation thus arises where the light weight, high stiffness and high surface area density of honeycombs could be explored simultaneously. The idea is to substantially reduce the overall weight/compactness of a structural system by using the load-bearing cellular structure to simultaneously perform the thermal management function.

In this paper, to optimize the cooling and structural load capacity of a two-dimensional cellular structure, the performance of a model system (Fig. 1) will be analyzed for various cell shapes and arrangements (Fig. 2). Here, a compact multi-chip module is cooled by forced convective flow across a core sandwiched between two heated skins (substrates). The scenario envisioned in Fig. 1 can be straightforwardly modified to cover the re-entry of a space vehicle consisting of sandwich shells, where the skin of the shell is actively cooled by fluid passing through its core. The optimization is built upon a previous heat transfer model for regular hexagonal cells subject to steady-state laminar flow with constant thermal/physical properties of both fluid and metal [5].

* Corresponding author.
E-mail address: tj121@eng.cam.ac.uk (T.J. Lu).

0017-9310/01/$ - see front matter
PII: S0017-9310(00)00234-9

Nomenclature

Bi	Biot number
c_a	proportional factor for surface area density
c_f	proportional factor for pressure drop
c_H	proportional factor for solid wall length
c_n	proportional factor for total number of slices over width W
c_p	specific heat
c_t	proportional factor for cell wall thickness
c_w	proportional factor for cell wall ends
D_h	hydraulic diameter
E	Young's modulus
G	in-plane shear modulus
h	local heat transfer coefficient
$\bar{h}$	overall heat transfer coefficient
H	heat sink height
k	thermal conductivity
I_1	thermal performance
I_2	thermomechanical performance index
l	cell wall length
L	heat sink length
L^*	characteristic length scale
$\dot{m}$	mass flow rate
M	heat sink weight
n	proportional factor for fin attachments
N_s	total number of slices over width W
Nu	Nusselt number
Δp	pressure drop
Pr	Prandtl number
q	heat flux
Q	total heat transfer rate
Re	Reynolds number
t	cell wall thickness
T	temperature
ΔT_m	logarithmic mean temperature difference
u	velocity
W	heat sink width

Greek symbols

γ	shear strain
ζ_i	curve-fitting parameter $(i = 1, 2, \ldots, t)$
μ	shear viscosity
ν	kinematic viscosity
ξ	local coordinates along cell walls
ρ	relative density
τ	shear stress
Ω	density

Subscripts

e	exit of heat sink
f	fluid
s	solid
w	substrate
0	inlet of heat sink

The cores in Fig. 1 are all arranged such that the cooling fluid passes along the axial direction of the cells. This arrangement differs from structural sandwich construction wherein, the cell axis is perpendicular to the skins. This design achieves large out-of-plane stiffness and strength but, is not amenable to cooling. The objective of this study is to discover cell shapes and arrangements that simultaneously optimize the structural and heat transfer performance at minimum weight. Two analytical models will be used. The micromechanical heat transfer model developed in [5] for regular hexagonal honeycombs is generalized to cover other cells, and, for convenience, is termed here as the 'corrugated wall model'. The second approach uses an 'effective medium model', that treats the cellular metal as a porous medium with effective thermal conductivity that depends on the cell morphology. Local volume averaging is utilized, subject to two-phase energy balance that addresses the local thermal non-equilibrium between the solid and fluid phases [6–8]. Exact solutions of the effective thermal conductivity are obtained for each type of cell shape (the interstitial heat transfer coefficients already exist in the open literature). Isothermal boundary conditions are assumed throughout, although the optimization is equally applicable to situations, where isoflux is more appropriate; the results on optimal cell shape and arrangement are not expected to change for the two cases. The in-plane shear moduli of the two-dimensional cellular solids are given in Appendix A.

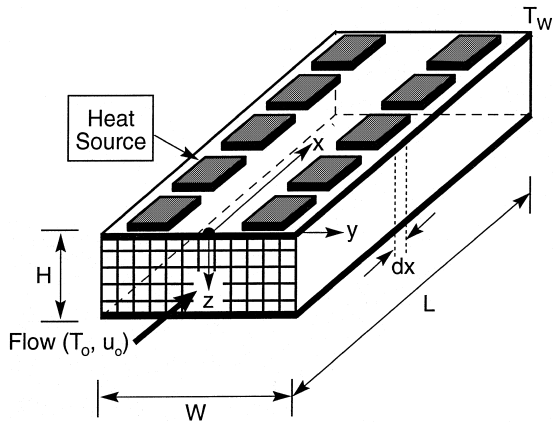

Fig. 1. Prototypical design of compact heat sink with two-dimensional metal honeycombs for cooling of multi-chip module by forced convection.

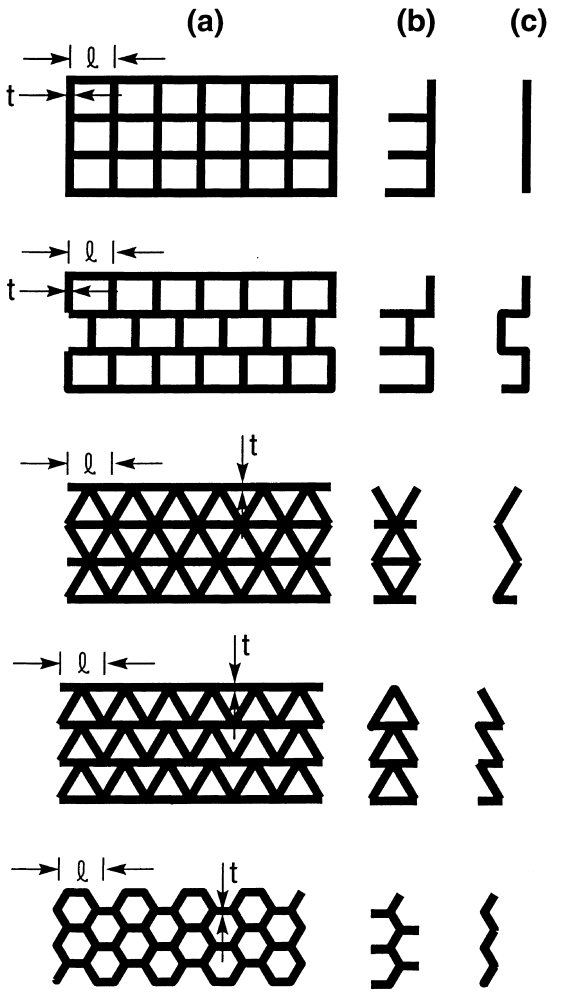

Fig. 2. Two-dimensional honeycombs analyzed: (a) cell shape and cell arrangement; (b) periodic cell (corrugated wall model); (c) corrugated wall without fin attachments.

2. Preliminary considerations

2.1. The model

Consider the prototypical compact heat exchanger design shown in Fig. 1, where the cooling is enhanced by forced convection across a two-dimensional metal array of thickness H sandwiched between two flat rectangular plates of length L and width W. The substrates are assumed to be thin and have large thermal conductivity so that the through-thickness heat conduction may be neglected. Both substrates are taken to be isothermal with uniform temperature T_w. The module is thermally insulated at the top ($z = 0$) and the bottom ($z = H$) by protective covers, and, without loss of generality, it is assumed that the sandwich structure is capped and thermally insulated at both ends ($y = \pm W/2$). Cooling fluid, with velocity u_0, temperature T_0 and pressure p_0, is forced into the cellular array at the inlet ($x = 0$). At the outlet ($x = L$), the temperature is T_e and the pressure p_e. The width of the channel, W, is assumed to be much larger than the cell size so that both the thermal and hydraulic fields are independent of the y-coordinate. Let Ω_f, ν_f, μ_f and c_p denote the fluid density, kinematic viscosity, shear viscosity and specific heat at constant pressure, respectively. The usual assumptions of steady-state laminar flow, and constant thermal/physical properties of both fluid and solid are made.

2.2. Cell morphology

The cellular array morphology is characterized by the cell size l, cell wall thickness t, relative density ρ (array density Ω^* divided by solid cell wall density Ω_s), and stacking order (Fig. 2(a)). It is assumed here that all cells have uniform wall thickness (although, cells having double-wall thickness can also be analyzed, as demonstrated in [5]). For simplicity, all cellular arrays are assumed to be perfect, free of process-induced geometrical imperfections. For the base cells considered (Fig. 2), it has been established that the cell wall aspect ratio, t/l, is dependent upon the relative density, ρ, as [1]

$$t/l = c_t(1 - \sqrt{1-\rho}), \tag{1}$$

where $c_t = 0.577, 1.0, 1.732$ for triangular, square and hexagonal cells, respectively. Eq. (1) can be easily converted to evaluate ρ for a given t/l. Similarly, the surface area density α_a for each cell shape is given by

$$\alpha_a = c_a \frac{\sqrt{1-\rho}}{l}, \tag{2}$$

where $c_a = 6.93, 4.0, 2.31$ for triangular, square and hexagonal cells, respectively. The corresponding hydraulic diameter, D_h, for each type of cell cross-section is

$$D_h \equiv 4\frac{1-\rho}{\alpha_a} = 4\frac{l\sqrt{1-\rho}}{c_a}. \tag{3}$$

It had been expected that the triangular system would be preferred on a heat dissipation basis, since it possesses the largest surface area for specified relative density and cell size. Later, this assertion will be contradicted since the performance will be judged on the basis of lowest weight for a specified thermal dispersion, Q, and pressure drop, Δp.

2.3. Effective thermal conductivity

The effective thermal conductivity of a two-dimensional cellular array is, in general, a second-order tensor [5,9,10]. The thermal conductivities, k_z in the z-direction normal to the substrate plane, and, k_y in the transverse direction, can be derived by analyzing heat conduction

across the periodic cell shown in Fig. 2b. The solutions expressed in terms of the solid conductivity, k_s and relative density, are

$$k_z = c_{kz}\rho k_s + (1-\rho)k_f \cong c_{kz}\rho k_s,$$
$$k_y = c_{ky}\rho k_s + (1-\rho)k_f \cong c_{ky}\rho k_s, \quad (4)$$

where the fluid thermal conductivity $k_f \ll k_s$ is assumed (which is valid for most fluid-saturated metal honeycombs), and c_{kz}, c_{ky} are proportionality coefficients accounting for the tortuous shape of the cell walls. For metal honeycombs operating at temperatures below 500°C, the contribution of thermal radiation to k_z and k_y is negligible [5,10]. Values for tortuosity coefficients, c_{kz} and c_{ky}, for the cells depicted in Fig. 2a are reported in Table 1. Note that they are bounded between 1/3 and 1/2 for all five geometries, consistent with results obtained by others [10,11]. It is noted that, due to the regularity of the structures, the lower and upper bounds coincide [11], such that the exact solutions are identical to those of Table 1.

2.4. Local heat transfer coefficient

For forced convective flow across a given cell, let h denote the local heat transfer coefficient averaged over the perimeter and let $Nu = hD_h/k_f$ denote the associated Nusselt number. For each duct shape, the dimensionless Nu is a function of the Reynolds number, $Re = u_f D_h/\nu_f$, and the Prandtl number, $Pr = c_p\mu_f/k_f$. When $Re < 2000$, the flow is laminar in the duct. For typical cellular arrays having cell sizes ~1 mm, this is a valid assumption under most circumstances. Laminar duct flow becomes fully developed after a distance, $x \approx 3D_h$, whereupon Nu becomes independent of the Reynolds number. For this study, the variation of Nu within the entrance length has been ignored, since for practical purposes: $L \gg D_h$. Accordingly, by invoking Eq. (3), the heat transfer coefficient h becomes

$$h = 0.25 c_a \frac{Nu\, k_f}{l\sqrt{1-\rho}}. \quad (5)$$

Values of Nu determined from numerical experimentation [9] for a uniform base temperature are independent of Pr, with $Nu = 2.35, 2.98, 3.35$ for triangular, square and hexagonal cells, respectively. The influence of cell cross-sectional shape on Nu is relatively small.

2.5. Pressure drop

For laminar flow, the pressure drop across the cellular array derived from the Hagen–Poiseuille solution of the momentum equation is given by the free stream velocity and the cell morphology by

$$\frac{\Delta p}{L} \equiv c_f \frac{4L}{D_h Re_{D_h}}\left(\frac{1}{2}\Omega_f u_*^2\right) = \frac{c_f c_a^2}{8}\frac{\Omega_f \nu_f u_0}{(1-\rho)^2 l^2}, \quad (6)$$

where $Re_{D_h} = u_* D_h/\nu_f$ is the Reynolds number, and $u_* = u_0/(1-\rho)$ is the fluid velocity averaged over the channel. The frictional coefficient is, $c_f = 14.17, 133, 15.07$ for square, triangular and hexagonal cells, respectively [9,12]. While the effect of cell shape on c_f is small, the pressure drop is significantly affected by shape because, from (6): $\Delta p \sim c_a^2$ (see Eq. (2)). Thus, while increasing the surface area density leads to an increase in the overall heat dissipation, there is an even larger increase in the pressure drop. Minimizing the pressure drop (6) while achieving a specified overall heat removal will be discussed in detail below.

2.6. In-plane shear modulus

As cores for load-bearing sandwich panels, the in-plane shear modulus G is of interest [1,14]. For example, under concentrated load, the panel deflects as a result of combined bending and shear deformation. The bending stiffness, S_B, at length L_p, in a direction normal to the cell axis, is [1,13]

$$\frac{1}{S_B} = \frac{2L_p^3}{B_1 E_p t_p W H^2} + \frac{L_p}{B_2 WHG}, \quad (7)$$

where E_p is the Young's modulus of the face sheets, t_p the sheet thickness and B_i $(i = 1, 2)$ are the bending coefficients that depend on the loading configuration [14]. In deriving (7), it has been assumed that $t_p \ll H$ such that thin facing sandwich beam theory applies (shear deformation due entirely to the cellular array core).

For the cellular arrays shown in Fig. 2a, the in-plane shear moduli at small ρ $(t \ll l)$ can be derived by extending the honeycomb model of Gibson and Ashby [1]

Table 1
Proportionality coefficients for five types of cell shape and cell arrangement

Cell type	c_a	c_{ky}	c_{kz}	c_H	n	Nu
Triangle-4	6.93	0.5	0.33	1.732	2.0	3.0
Triangle-6	6.93	0.5	0.5	1.155	3.0	3.0
Square-3	4.0	0.5	0.4	1.5	1.778	3.614
Square-4	4.0	0.5	0.5	1.0	2.0	3.614
Hexagon	2.31	0.5	0.5	1.155	1.5	4.021

(Appendix). The in-plane shear modulus of an array of square cells with connectivity of 4 is

$$G/E_s = (1/2)(t/l)^3, \tag{8a}$$

where E_s is the Young's modulus of the cell wall material. For square cells with connectivity of 3,

$$G/E_s = (4/5)(t/l)^3. \tag{8b}$$

For regular hexagonal cells,

$$G/E_s = (1/\sqrt{3})(t/l)^3. \tag{8c}$$

For triangular cells with connectivity of 4,

$$G/E_s = 89(t/l)^3, \tag{8d}$$

and for triangular cells with connectivity of 6,

$$G/E_s = (\sqrt{3}/4)(t/l). \tag{8e}$$

Among the arrays shown in Fig. 2a, the triangular structure with connectivity 6 has the greatest stiffness (at a specified relative density). It also has in-plane isotropy, whereas square arrays are highly anisotropic and hexagons are extremely compliant [1]. Triangular systems with connectivity 6 deform by cell-wall stretching under in-plane shear. All other cellular arrays of Fig. 2a deform by cell-wall bending. This difference in deformation mechanisms is reflected in the linear dependence of G upon ρ for the triangular cells, and by the non-linear power law dependence of G upon ρ for all other structures.

3. Corrugated wall model

3.1. Heat loss from a single-corrugated wall with fins

The problem shown in Fig. 1 is significantly simplified if the heat sink is divided into periodic slices of equal width, as illustrated in Fig. 2b for each base cell geometry. It is apparent from Fig. 2b that each slice consists of a corrugated wall (Fig. 2(c)), with or without fin attachments. Therefore, following [5], a two-step approach is adopted to solve for the thermal fields. In the first step, the analysis of heat transfer is performed for the corrugated walls by excluding the effects of fins. Then, the contribution from the fins is added, where appropriate.

In the absence of fin attachments, the governing equation of temperature T along the length of a single-corrugated wall (Fig. 3) is

$$\frac{d^2T}{d\xi^2} - \frac{2h}{k_s t}(T - T_f) = 0, \tag{9}$$

where $T_f(x)$ is the *mean* fluid temperature at location x (to be determined next) and ξ is the local coordinate

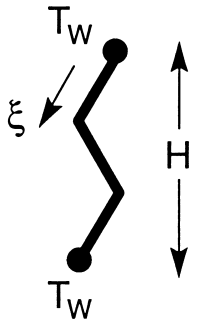

Fig. 3. A single-corrugated wall (without fin attachments), with local coordinate and isothermal boundary conditions.

along the wall with the origin $\xi = 0$ coinciding with $z = 0$, and $\xi = c_H H$ at $z = H$. The values of the tortuous coefficient c_H are given in Table 1. The effects of radiation at the wall surface can be shown to be small, and hence is neglected in the derivation of Eq. (9). Subjected to the boundary conditions that $T = T_w$ at $\xi = 0$ and at $\xi = c_H H$, Eq. (9) can be solved to arrive at

$$T(x,\xi) = T_f(x) + (T_w - T_f(x))\frac{\cosh\left[\sqrt{Bi/2}(c_H H - 2\xi)/t\right]}{\cosh(\sqrt{Bi/2}c_H H/t)}, \tag{10}$$

where $Bi = ht/k_s$ is the Biot number. It is expected that $Bi \ll 1$ for typical cellular metal arrays with $t \sim 10^{-1}$ mm.

The heat lost to the cooling medium per unit length of the corrugated wall is

$$q_1 = -2k_s t\left.\frac{dT}{d\xi}\right]_{\xi=0} = 2\sqrt{2Bi}k_s(T_w - T_f)\tanh\left(\sqrt{Bi/2}c_H H/t\right). \tag{11}$$

The contribution of heat loss from fin attachments for regular hexagonal cells has been analyzed in [5] using both exact and approximate solutions. It was found that the approximate solution for the total heat loss with fin attachments, $q \cong 1.5q_1$, closely describes the exact (but much more complicated) solution. Here, the same strategy as that used in [5] is extended to cover other types of base cell. The approximate solution for the total heat loss from a single-corrugated wall and its fin attachments can be written as

$$q = nq_1 = 2n\sqrt{2Bi}k_s(T_w - T_f)\tanh\left(\sqrt{Bi/2}c_H H/t\right), \tag{12}$$

where n is a correction coefficient accounting for the contribution of fins. For each base cell, n is reported in Table 1.

3.2. Mean fluid temperature

Following [5], a simple model is used to solve for the steady-state distribution of the average fluid temperature inside the heat sink, with the assumption that the heat transfer between the fluid and solid cell wall is governed by a constant heat transfer coefficient obtained from laminar duct flow, Eq. (5). As is customary in the heat transfer analysis of a duct, a mean temperature $T_f(x)$ of the fluid is defined over the cross-section of the cellular array (at location x = fixed), such that for the control volume of length dx:

$$\dot{m}c_p[T_f(x+\mathrm{d}x) - T_f(x)] = N_s q(x) + q_w(x), \tag{13}$$

where $\dot{m} = \Omega_f v_0 HW$ is the mass flow rate at the entrance to the heat sink, $N_s = c_n W/l$ is the total number of slices over width W, and

$$q_w(x) = 2h(W - N_s c_w t)[T_w - T_f(x)], \tag{14}$$

is the heat flux into the fluid from both face sheets. Here, $c_n = 2/3$ for hexagonal cells and $c_n = 1$ for all other base cells: whereas $c_w = 1$ for square cells and $c_w = \sqrt{3}/2$ for all other base cells. Notice that T_f calculated from Eq. (14) is the average (local) temperature that satisfies the First Law of Thermodynamics.

Combination of Eqs. (12)–(14) gives rise to an ordinary differential equation for the mean fluid temperature $T_f(x)$. The solution is

$$T_f(x) = T_w - (T_w - T_0)\exp(-x/L^*), \tag{15}$$

where L^* is the characteristic length scale given by

$$L^* = \frac{\Omega_f c_p u_0 H}{2h}\left[1 - \frac{c_n c_w t}{l} + \frac{c_n nt}{l}\sqrt{\frac{2}{Bi}}\tanh\left(\sqrt{Bi/2}\,c_H H/t\right)\right]^{-1}. \tag{16}$$

From Eq. (15), the average fluid temperature inside the heat sink is obtained as

$$\bar{T}_f = T_0 + (T_w - T_0)\left\{1 - \frac{L^*}{L}[1 - \exp(-L/L^*)]\right\}. \tag{17}$$

Notice that in the limit $L/L^* \to \infty$, $\bar{T}_f \to T_w$ as expected.

3.3. Overall heat transfer coefficient

The total heat dissipated from the sandwich structure is $Q = \dot{m}c_p(T_e - T_0)$ which, by noting that $T_e = T_f(L)$, becomes

$$Q = \Omega_f u_0 c_p HW(T_w - T_0)\{1 - \exp(-L/L^*)\}. \tag{18}$$

The overall heat transfer coefficient, $\bar{h}$, of the heat sink is defined as [5,10]

$$\bar{h} = \frac{Q}{2LW\Delta T_m}, \tag{19}$$

where ΔT_m is the logarithmic mean temperature difference:

$$\Delta T_m = \frac{(T_w - T_0) - (T_w - T_e)}{\ln[(T_w - T_0)/(T_w - T_e)]}. \tag{20}$$

It can be readily verified that $\Delta T_m = T_w - \bar{T}_f$. The resulting expression for $\bar{h}$ is

$$\frac{\bar{h}}{h} = 1 - \frac{c_n c_w t}{l} + \frac{c_n nt}{l}\sqrt{\frac{2}{Bi}}\tanh\left(\sqrt{Bi/2}\,c_H H/t\right), \tag{21a}$$

or, equivalently,

$$\bar{h} = 0.25\frac{c_a Nu\, k_f}{l\sqrt{1-\rho}}\left[1 - \frac{c_n c_w t}{l} + 2c_n n\sqrt{\frac{2k_s t\sqrt{1-\rho}}{c_a Nu\, k_f l}}\tanh\left(\frac{c_H H}{2l}\sqrt{\frac{c_a Nu\, k_f l}{2k_s t\sqrt{1-\rho}}}\right)\right]. \tag{21b}$$

4. Effective medium model

In this model, the governing equations for the velocity and temperature fields in the fluid-saturated porous medium are derived by using the volume-averaging method [6–8]. The properties of each phase are averaged separately within a representative unit element (i.e., individual cells) and correlated with bulk properties of the pure phases. The representative unit volume has a surface area per unit volume, a_a, local heat transfer coefficient, h, and effective thermal conductivity, k_z. The energy equation governing the temperature in the solid phase, $T(x,z)$ after reaching steady-state may then be written as

$$\frac{\mathrm{d}^2 T}{\mathrm{d}z^2} - \alpha_a \frac{h}{k_z}(T(x,z) - T_f(x)) = 0, \tag{22}$$

where it has been assumed that most of the heat flux through the solid is normal to the fluid flow (i.e., $|\partial T/\partial z| \gg |\partial T/\partial x|$). Upon defining $\chi^2 = h\alpha_a/k_z$, the cell wall temperatures in the heat sink shown in Fig. 1 are determined as ($T < T_f$)

$$T(x,z) = T_f(x) + (T_w - T_f(x))\frac{\cosh[\chi(H/2 - z)]}{\cosh(\chi H/2)}. \tag{23}$$

Local energy balance on the fluid phase for a representative control volume, height H, gives

$$q = \Omega_f c_p u_0 HW\frac{\mathrm{d}T_f}{\mathrm{d}x} = h\alpha_a HW(T_w - T_f)\eta, \tag{24}$$

where $\eta = \tanh(\chi H/2)/(\chi H/2)$ denotes the effective fin efficiency.

When the fluid is everywhere cooler than the solid, the mean fluid temperature is the same as Eq. (15), but with the characteristic length scale, L^*, given by

$$L^* = \frac{\Omega_f c_p u_0}{h\alpha_a \eta}. \tag{25}$$

Following the same procedure that leads to Eqs. (21a) and (21b) in the corrugated wall model, the overall heat transfer coefficient for the effective medium model is obtained as

$$\bar{h} = \frac{c_a}{2l}\sqrt{Nu\,k_f c_{kz} k_s \rho}\tanh\left(\frac{c_a H}{4l}\sqrt{\frac{Nu\,k_f}{c_{kz}k_s\rho}}\right). \tag{26}$$

5. Design optimizations

The intent of this section is mainly two fold: (i) to compare the predictions from the two analytical models, and (ii) to define non-dimensional indices for heat dissipation, pressure drop and stiffness that facilitate selection of cell morphologies and heat sink dimensions which maximise heat dissipation (and stiffness) at specified pressure drop. Such optimizations are subject to two important provisos. The first is that the morphological representation developed in Section 2 applies over the ranges of cell size and relative density embraced by the included formulae. The second is that the flow remains laminar and fully developed, both thermodynamically and thermally, such that the local heat transfer can be represented by Eq. (5) and the pressure drop by Eq. (6).

5.1. Corrugated wall model versus effective medium model

The heat transfer performance of a heat sink is commonly gauged by the ratio of total heat transfer rate to the pumping power needed to force the fluid through: the higher this ratio, the better the heat sink performance. A non-dimensional scaling index I_1 is thence introduced as

$$I_1 = c_1 \bar{h}/\Delta p, \tag{27}$$

where $c_1 = v_f \Omega_f u_0/k_s$. For the corrugated wall model, it can be shown that

$$I_1 = \frac{2Nu\,k_f(1-\rho)^{3/2} l}{c_f c_a k_f L}\left\{1 - c_n c_w c_t(1-\sqrt{1-\rho}) + c_n n\sqrt{\frac{8k_s c_t(1-\sqrt{1-\rho})\sqrt{1-\rho}}{Nu\,c_a k_f}}\tanh\left(\frac{c_H H}{l}\sqrt{\frac{Nu\,c_a k_f\sqrt{1-\rho}}{8k_s c_t(1-\sqrt{1-\rho})}}\right)\right\}. \tag{28a}$$

Similarly, for the effective medium model,

$$I_1 = \frac{2l(1-\rho)^2}{c_f c_a k_f L}\left\{\sqrt{Nu\,k_f c_{kz} k_s \rho}\tanh\left(\frac{c_a H}{2l}\sqrt{\frac{Nu\,k_f}{c_{kz}k_s\rho}}\right)\right\}. \tag{28b}$$

Both the corrugated wall model and the effective medium model are employed below to investigate the effects of cell morphology on heat transfer efficiency. For the base cells of Fig. 2, the relevant proportionality coefficients are listed in Table 1. For regular hexagonal structures, the predicted heat transfer efficiency I_1 against ρ from both models are shown in Fig. 4 for $k_s = 200$ W/m K (typical of aluminum), $k_f = 0.026$ W/m K (air at 300 K), $l = 1$ mm, $H/l = 10$, and $L/l = 100$. Although the two models exhibit the same general trend, the predicted I_1 from the corrugated wall model is consistently higher than that from the effective medium model. The discrepancy is mainly due to the extra heat dissipation from the plate surfaces and fin attachments that are ignored in the effective medium model. In the corrugated wall model, these are separately accounted for by the $1 - c_n c_w c_t(1-\sqrt{1-\rho})$ term and the coefficient $n(>1)$ in Eq. (28a). The effect of heat transfer across the plate surfaces on the overall heat transfer coefficient is small, as can be seen from Fig. 4, where the prediction of Eq. (28a) without the $1 - c_n c_w c_t(1-\sqrt{1-\rho})$ term is plotted. However, if this term is retained and $n = 1$ is assumed (heat transfer due to fin attachments ignored), the knock down effect on $\bar{h}$ and hence on I_1 is quite significant (Fig. 4). If both effects are ignored, then the predicted I_1 from the corrugated wall model correlate well with those predicted from the

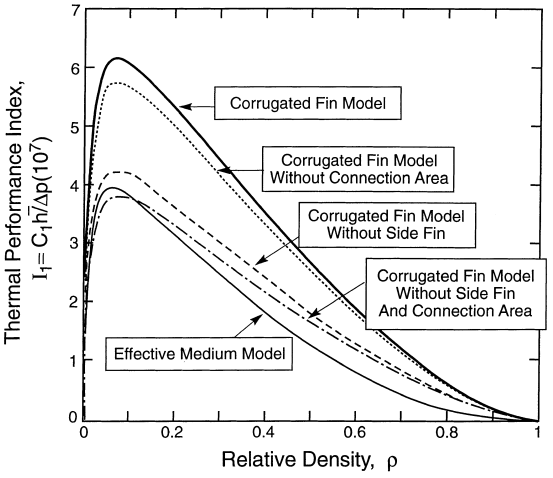

Fig. 4. Thermal performance index I_1 plotted as a function of relative density for hexagonal structure. The parameters used are $l = 1$ mm, $H/l = 10$, $L/l = 100$, $k_s = 200$ W/mK and $k_f = 0.026$ W/m K.

effective medium model. Unless otherwise stated, all the results presented below are calculated from the corrugated wall model.

5.2. Optimal cell morphology for maximum thermal performance

The predicted heat transfer efficiency I_1 against ρ from the corrugated wall model are shown in Fig. 5 for each base cell (the parameters are identical to those selected for Fig. 4). The results illustrate that, amongst the five different cellular structures considered, the regular hexagonal system produces the best heat transfer efficiency, at specified relative density, cell size and heat sink dimensions. The triangular cells are the least efficient. Even though the triangular system has the largest surface area density at specified relative density and cell size and hence, the largest heat dissipation capability ($\bar{h} \sim c_a$, Eq. (21b) or (26)), it has an even larger pressure drop ($\Delta p \sim c_a^2$, Eq. (6)). Accordingly, the heat transfer efficiency index I_1 is *inversely proportional to the shape factor*: $c_a = 2.31, 4.0, 6.93$ for hexagonal, square and triangular cells, respectively. This can be seen explicitly from either Eq. (28a) or (28b).

For each cell and for the parameters listed afore, the thermal performance index I_1 increases steeply with increasing ρ, reaches a maximum, I_1^{max}, and then decreases. The relative density, ρ_{opt}, at I_1^{max} is dependent upon H/l and other parameters to be specified below. This general trend remains unchanged if parameters other than those used for plotting Figs. 4 and 5 are used.

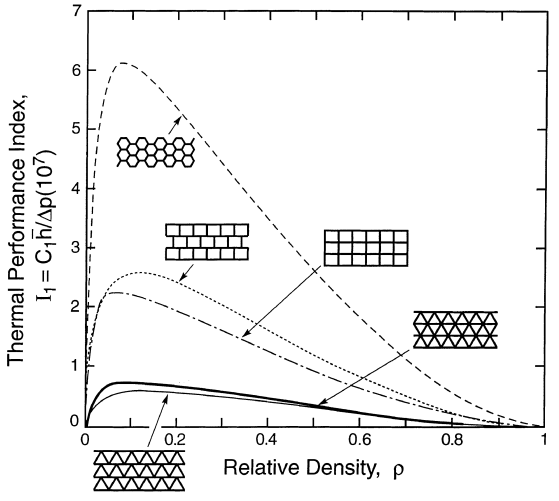

Fig. 5. Thermal performance index I_1 plotted as a function of relative density for triangular, square and hexagonal structures. The corrugated wall model is used for the plotting, with $l = 1$ mm, $H/l = 10$, $L/l = 100$, $k_s = 200$ W/mK and $k_f = 0.026$ W/m K.

5.3. Optimal systems for thermal performance

The maximum values of the index, I_1^{max}, and the corresponding relative densities, ρ_{opt}, are plotted in Fig. 6 as functions of H/l. The parameters are identical to those selected for plotting Fig. 4. The heat dissipation capacity increases rapidly as H/l increases up to about 20. Thereafter, it reaches an asymptotic limit. This behavior arises because, when H/l is sufficiently large (at specified T_w), most of the heat has already been dissipated before it reaches the center of the core ($z = H/2$ in Fig. 1). It is therefore unnecessary to unduly increase the heat sink height in order to increase heat dissipation: just as it is no longer necessary to increase the heat sink length beyond $L = 3L^*$ when the fluid temperature $T_f(L)$ has already approached the target temperature T_w. The asymptotic values are quite sensitive to the cell topology, with the largest values arising for the hexagons. One implication is that (for a specified pressure drop), there is a *maximum amount of heat that can be dissipated by each cell topology*. Consequently, in high heat flux situations, only hexagons can satisfy the thermal requirements.

The optimal relative density ρ_{opt} increases upon increasing H/l (Fig. 6b). Moreover, when I_1^{max} reaches its asymptotic level, this density is independent of the base cell $\rho_{opt} \approx 0.24$. This relatively large ρ_{opt} indicates that heat transfer is maximized when convective heat transfer

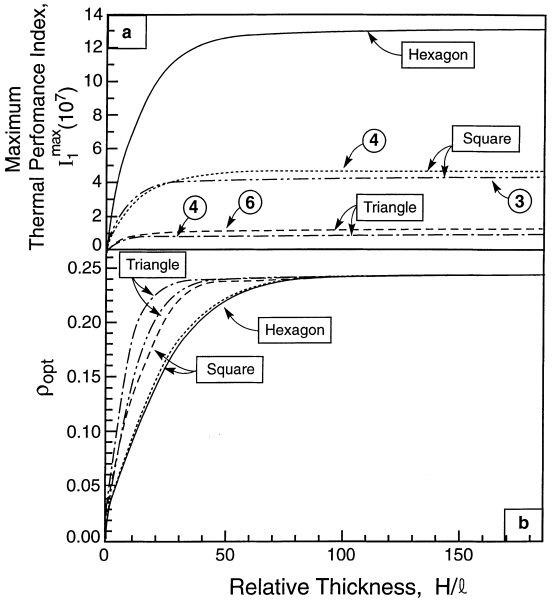

Fig. 6. (a) The maximum thermal performance index I_1^{max}; (b) the corresponding optimal relative density ρ_{opt} plotted as a function of normalized heat sink height H/l. The corrugated wall model is used for the plotting, with $l = 1$ mm, $L/l = 100$, $k_s = 200$ W/m K and $k_f = 0.026$ W/m K.

interacts favorably with heat conduction along cell walls. To facilitate subsequent analysis, the dependencies of $I_1^{\max}$ and ρ_{opt} on H/l have been approximated by:

$$I_1^{\max} \cong \zeta_1 \tanh(\zeta_2 H/l), \tag{29a}$$

$$\rho_{\text{opt}} \cong 0.24 \tanh(\zeta_3 H/l), \tag{29b}$$

where $\zeta_1 = (12.88, 4.598, 4.096, 1.075, 0.724) \times 10^{-7}$, $\zeta_2 = 0.045, 0.043, 0.07, 0.07, 0.125$, and $\zeta_3 = 0.032, 0.035, 0.048, 0.065, 0.09$ for hexagonal, four-connected square, three-connected square, six-connected triangle and four-connected triangle, respectively.

These results may be used to guide the design of a lightweight compact heat sink. For this purpose, the optimal thickness of the heat exchanger is first chosen from Fig. 6a to provide the thinnest sandwich structure that achieves the required thermal performance index $I_1^{\max}$. Then, the optimal relative density of the cellular core is selected from Fig. 6b. Thereupon, the weight of the heat sink ($\bar{M} = \rho_{\text{opt}} \Omega_s HLW$), is given by:

$$\frac{\bar{M}}{\Omega_s LWl} \equiv \rho_{\text{opt}} \frac{H}{l} \approx \frac{0.24}{\zeta_2} \tanh\left[\frac{\zeta_3}{\zeta_2} \tanh^{-1}\left(\frac{I_1^{\max}}{\zeta_1}\right)\right] \times \tanh^{-1}\left(\frac{I_1^{\max}}{\zeta_1}\right). \tag{30}$$

Fig. 7 plots the normalized weight ($\bar{M}/\Omega_s LWl$) against $I_1^{\max}$. This plot reaffirms that high levels of heat dissipation (at specified pumping power) are inaccessible for

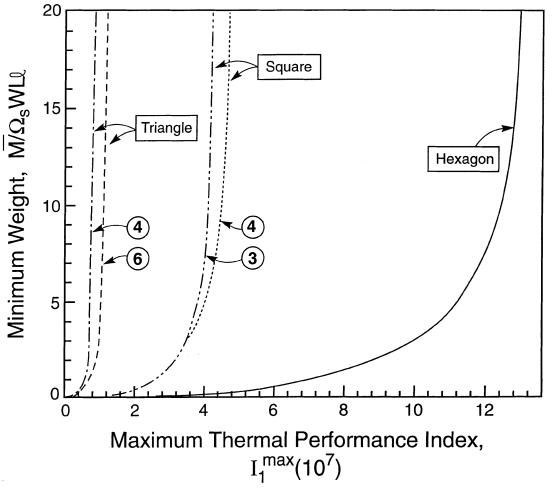

Fig. 7. Normalized heat sink minimum weight $\bar{M}/\Omega_s LWl$ plotted as a function of the maximum thermal performance index $I_1^{\max}$. The heat sink is made of 2D cellular systems having optimal relative densities, ρ_{opt}. The corrugated wall model is used, with $l = 1$ mm, $L/l = 100$, $k_s = 200$ W/m K and $k_f = 0.026$ W/m K.

triangular and square cells. Specifically, at the limit $\rho_{\text{opt}} = 0.24$, hexagonal cells dissipate about three times more heat than square cells, and about 12 times that achievable with triangular cells. Moreover, hexagonal cells invariably provide specified levels of heat dissipation at lowest weight.

5.4. Optimal systems for thermomechanical performance

It would be of great interest to find the lightest structure that achieves a specified heat dissipation, while sustaining a defined structural load. Such an optimization is beyond the scope of this article. Instead a simple, though arbitrary, metric is chosen that allows some aspects of the interplay to be explored. The basis for the loading parameter is the recognition that core shear has a major influence on the minimum weights realized in practice [14,15]. Accordingly, the non-dimensional in-plane shear stiffness, G/E_s, is taken as a relevant measure of the structural utility. The convolution of load bearing with heat dissipation is assumed to be reflected in the product of this shear stiffness with the heat dissipation/pressure drop index, I_1, resulting in a new dimensionless index:

$$I_2 \equiv (G/E_s) I_1 = c_1 \frac{G}{E_s} \frac{\bar{h}}{\Delta p}. \tag{31}$$

This index has an implicit dependence on ρ, through both G/E_s and I_1.

For assessment of lowest overall weight, it is noted that sandwich panels optimized for load bearing have explicit requirements on core thickness [15]. Accordingly, a peak value of the index I_2, denoted $\hat{I}_2$, is sought for specified H/l:

$$\hat{I}_2 = (G/E_s) I_1|_{H/l}. \tag{32}$$

The trend in $\hat{I}_2$ with H/l is plotted in Fig. 8. The results can be conveniently expressed as

$$\hat{I}_2 \cong \zeta_4 [\tanh(\zeta_5 H/l)]^{\alpha}, \tag{33}$$

where the coefficients $\alpha = 4.3, 2.2, 3.5, 3.9, 3.6$, $\zeta_4 = (8.15, 3.45, 2.15, 0.49, 0.69) \times 10^{-9}$ and $\zeta_5 = 0.034, 0.07, 0.09, 0.036, 0.033$ for hexagonal, six-connected triangular, four-connected triangular, four-connected square and three- connected square cells, respectively. In this plot, each H/l has an implicit relative density, ρ_{opt} (Fig. 6). The implication of Fig 8 is that for designs requiring thin cores (small $H/l < 25$), panels with six-connected triangular cells outperform all other structures, because of their superior load-bearing characteristics. The situation changes at large $H/l (> 25)$, where the hexagonal cells outperform all others because of their superior thermal performance (Fig. 8). These characteristics reveal that interesting nuances are to be

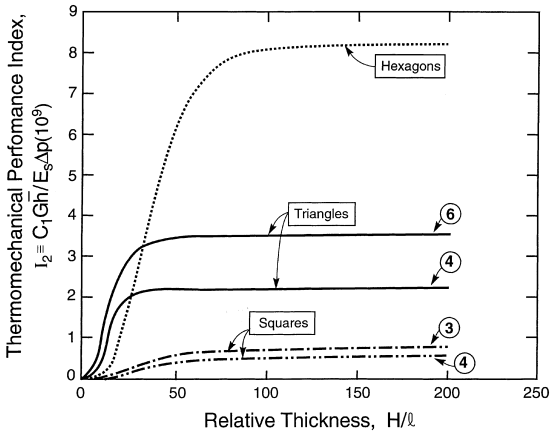

Fig. 8. Thermomechanical performance index $\hat{I}_2$ plotted as a function of core thickness for triangular, square and hexagonal structures at optimal relative density ρ_{opt}. The corrugated wall model is used for the plotting, with $l = 1$ mm, $L/l = 100$, $k_s = 200$ W/m K and $k_f = 0.026$ W/m K.

expected when joint optimization for both structural loads and heat dissipation are attempted.

Since ρ_{opt} is implicit in Fig 8, the structural weight exhibits similar characteristics, as illustrated in Fig 9, where the normalized weight, $\bar{M}/\Omega_s LWl$, has been plotted against $\hat{I}_2$. Note that, to a good approximation, Fig. 9 can be represented by

$$\frac{\bar{M}}{\Omega_s LWl} \approx \frac{0.24}{\zeta_5} \tanh\left[\frac{\zeta_3}{\zeta_5}\tanh^{-1}\left(\frac{\hat{I}_2}{\zeta_4}\right)^{1/\alpha}\right] \times \tanh^{-1}\left(\frac{\hat{I}_2}{\zeta_4}\right)^{1/\alpha}. \quad (34)$$

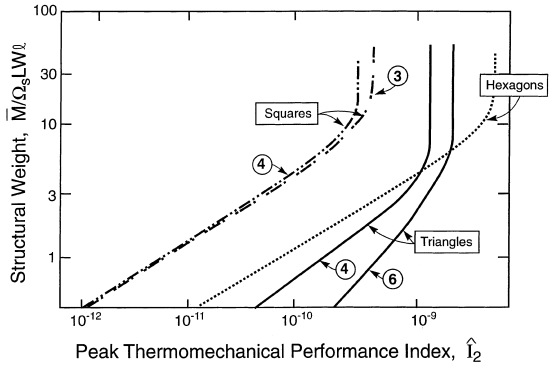

Fig. 9. Normalized heat sink minimum weight $\bar{M}/\Omega_s LWl$ plotted as a function of thermomechanical performance index $\hat{I}_2$ at optimal relative density ρ_{opt}. The corrugated wall model is used, with $l = 1$ mm, $L/l = 100$, $k_s = 200$ W/m K and $k_f = 0.026$ W/m K.

It is to be recalled that, in both Eq. (34) and in Fig. 9, the core thickness, H/l, is implicit, through Eq. (33).

6. Conclusion

Two analytical models are used to describe the characteristics of heat transfer in two-dimensional structures with forced convection. The corrugated wall approach models the detailed cellular structure, whilst the effective medium model uses volume averaging techniques. Both models are able to predict the thermal fields as functions of cell morphology and flow parameters: although the effective medium model somewhat underestimates the heat dissipation due to the assumption that the conduction of heat occurs predominantly normal to the convective flow. The solutions have been applied to a variety of cell structures, including square cells with connectivity of either three or four, triangular cells with connectivity of either six or four, and regular hexagonal cells.

Two dimensionless scaling indices are introduced to help identify the optimal cell shape and arrangement. The first is based on the ratio of overall heat transfer coefficient to pumping power, and the other combines thermal performance with shear stiffness. Hexagonal structures are found to provide the best heat transfer efficiency, whereas triangular systems are the least efficient (even though the latter have the largest surface area density). For a specified relative density, cell size and heat sink dimensions, the triangular material may dissipate, say, twice as much heat as the hexagonal, but the pumping power needed to achieve this quadruples. Furthermore, for a specified pumping power, there is a maximum amount of heat that can be dissipated by each cell topology: such that the highest levels of heat dissipation with hexagonal cells are not accessible for triangular and square cells. For all cell topologies, the relative density corresponding at the maximum heat dissipation is about 0.24, indicating the importance of heat conduction along cell walls.

If the heat sink is required to carry structural load as well as dissipate heat, then for small core thickness/low heat flux scenarios the six-connected triangular cells provide the best overall performance, because their high stiffness compensates more than for their inferior heat dissipation capability. Conversely, in high heat flux situations where relatively thick cores are required, hexagonal cells have the best overall performance.

Acknowledgements

This work is supported by EPSRC, UK and by the ARPA/ONR MURI program on Ultralight Metal

Structures, USA (No. N00014-1-96-1028). TJL also wishes to thank Dr. C. Chen for carrying out the finite element calculations, and Dr. A.-F. Bastawros for helpful discussions.

Appendix A. Calculation of in-plane shear modulus

The in-plane shear stiffness of a periodic two-dimensional cellular structure with regular hexagonal cells has been studied by Gibson and Ashby [1], and is given in Eq. (8e). For cellular structures having other base cells, their in-plane shear stiffness are derived below.

A.1. Square with connectivity of 4

Consider the deformation of the unit cell under shear stress τ as shown in Fig. 10(a). By symmetry, there is no relative motion of the points A, C and O. The shearing deflection of the structure is due to the bending of beams BO and DO and their rotation about the point O. Since all the joints rotate through an angle ϕ, by using the standard result for beam deflection $\delta = Ml^2/6E_sI$ with $I = t^3/12$, one has

$$\phi = \frac{\tau}{E_s}\left(\frac{l}{t}\right)^3. \tag{A1}$$

The shearing defection of point B with respect to O is

$$\bar{u} = \frac{\tau l}{3E_S I}\left(\frac{l}{2}\right)^3 + \phi\frac{l}{2} = \frac{\tau l^4}{E_s t^3}. \tag{A2}$$

The shear strain, γ, is given by

$$\gamma = \frac{2\bar{u}}{l} = \frac{2\tau}{E_s}\left(\frac{l}{t}\right)^3, \tag{A3}$$

from which the shear modulus $G = \tau/\gamma$ is obtained as

$$\frac{G}{E_s} = \frac{1}{2}\left(\frac{t}{l}\right)^3. \tag{A4}$$

A.2. Square with connectivity of 3

Consider the deformation of the unit cell under shear stress τ as shown in Fig. 10b. By symmetry, there is no relative motion of the points A, C, E, F and O. The shearing deflection of the structure is due to the bending of beams BE and DF and their rotation about the points F and E, respectively. All the joints rotate through an angle ϕ. Then, from the standard beam bending results, $\phi = (Ml/2)/24E_sI$, we obtain

$$\phi = \frac{\tau}{4E_s}\left(\frac{l}{t}\right)^3. \tag{A5}$$

The shearing defection of point B with respect to E is

$$\bar{u} = \frac{\tau l}{3E_s I}\left(\frac{l}{2}\right)^3 + \phi\frac{l}{2} = \frac{5\tau l^4}{8E_s t^3}. \tag{A6}$$

The shear strain, γ, is given by

$$\gamma = \frac{2u_s}{l} = \frac{5\tau}{4E_s}\left(\frac{l}{t}\right)^3, \tag{A7}$$

from which the shear modulus $G = \tau/\gamma$ is obtained as

$$\frac{G}{E_s} = \frac{4}{5}\left(\frac{t}{l}\right)^3. \tag{A8}$$

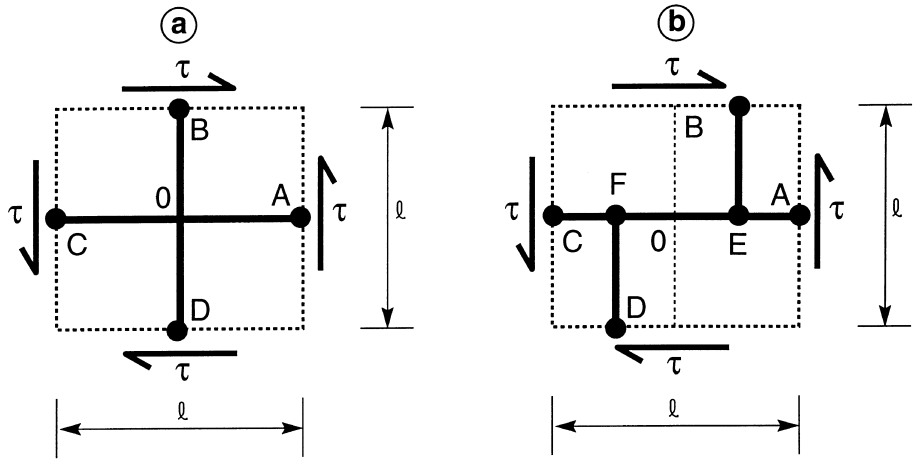

Fig. 10. Unit cell of square honeycomb with connectivity of (a) 4, (b) 3, subject to in-plane shear.

A.3. Triangle with connectivity of 6

The in-plane Young's modulus of the triangular system with connectivity of 6 is [1,12]:

$$\frac{E}{E_s} = \frac{2}{\sqrt{3}}\left(\frac{t}{l}\right). \tag{A9}$$

Since this structure is isotropic, the corresponding in-plane shear modulus can be directly calculated from $G = E/2(1+v)$, as

$$\frac{G}{E_s} = \frac{\sqrt{3}}{4}\left(\frac{t}{l}\right), \tag{A10}$$

where $v = 1/3$ has been used [1,12].

A.4. Triangle with connectivity of 4

For a triangular system with connectivity of 4, it is difficult to calculate its in-plane shear modulus using the above simple beam theory and the extensions. The method of finite elements is used instead. Details of the finite element method as applied to two-dimensional cellular structures can be found in [3,10]. In the finite element model, a structure of size $L_x \times L_y$ is taken as the unit cell of an infinite triangular system; a uniform cell-wall thickness t across the entire structure is assumed. Periodic boundary conditions are applied. The relative density of the structure studied is then given by

$$\rho = \frac{t\sum l_k}{L_x L_y}, \tag{A11}$$

where l_k are the cell-wall lengths and the sum is carried over the total number of cell walls in the unit cell. In the finite element analysis, each cell edge is modeled by Timoshenko beam elements (B22 beam element in the finite element code ABAQUS); the relative density of the structure is changed by changing the cell-wall thickness. In order to get satisfactory results, the beam element length in the finite element model is about 2 and 4 times of its thickness when the relative density is 22% and 10%, respectively. Fig. 11 plots the predicted in-plane shear stiffness as a function of ρ, which can be accurately described by the following curve-fitting relationship:

$$\frac{G}{E_s} = 2.143\,\rho^3. \tag{A12}$$

The results presented in Fig. 11 are calculated with $L_x/l = 25$ and $L_x/l = 10$ (i.e., the total number N of cells in the finite element mesh is 250); a mesh sensitivity study has established that these do not change as N is increased or decreased. Combining Eq. (A12) with Eq. (1), one recovers, at small ρ, Eq. (8e). Note that, in contrast to the stiff triangular structure with connectivity of 6, where deformation is dominated by cell wall stretching, a four-connected triangular structure deforms by cell wall bending and hence is much more compliant.

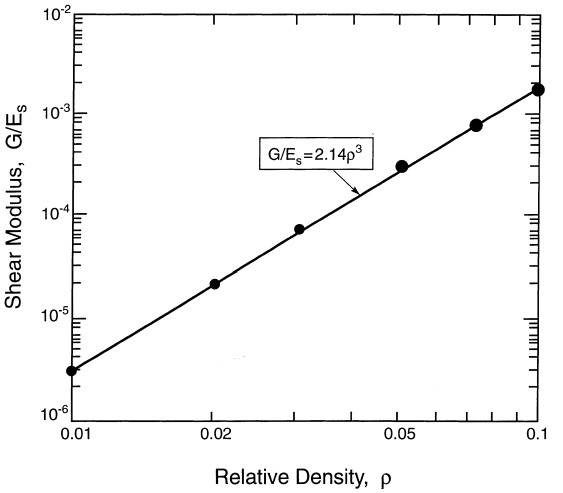

Fig. 11. In-plane shear modulus G of square honeycomb with connectivity of either 3 or 4 plotted as a function of relative density.

The in-plane shear moduli of cellular structures with square cells having connectivity of either 4 or 3 have also been calculated by the finite element method, and are presented in Fig. 12. The analytical predictions, Eqs. (A4) and (A8), are included in Fig. 12 for comparison; excellent agreement between analytical and finite element results is obtained.

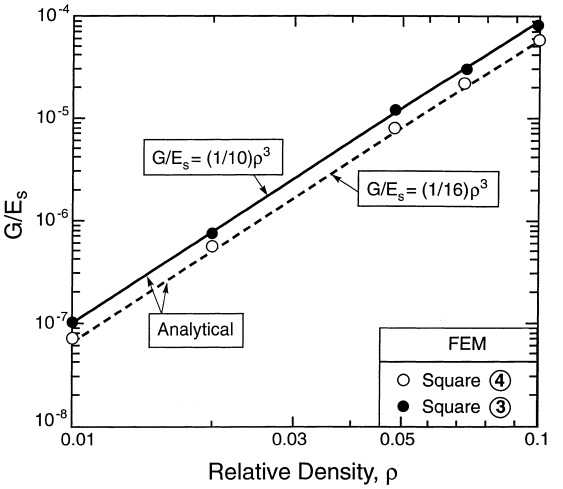

Fig. 12. In-plane shear modulus G of triangular honeycomb with connectivity of 4 plotted as a function of relative density.

References

[1] L.J. Gibson, M. Ashby, Cellular Solids: Structure and Properties, second ed., Cambridge University Press, New York, 1997.

[2] T.J. Lu, H.A. Stone, M.F. Ashby, Heat transfer in open-cell metal foams, Acta Mater. 46 (1998) 3619–3635.

[3] C. Chen, T.J. Lu, N.A. Fleck, Effect of imperfections on the yielding of two-dimensional foams, J. Mech. Phys. Solids 47 (1999) 2235–2272.

[4] A.-F. Bastawros, A.G. Evans, J. Cochran, Modeling and optimization of heat dissipation in stiff sandwich panels with two-dimensional cellular metal cores, in press.

[5] T.J. Lu, Heat transfer efficiency of metal honeycombs, Int. J. Heat Mass Transfer 42 (1999) 2031–2040.

[6] J.C.Y. Koh, R. Colony, Analysis of cooling effectiveness for porous material in a cooling passage, J. Heat Transfer 96 (1974) 324–330.

[7] K. Vafai, M. Sozen, Analysis of energy and momentum transport for fluid flow through a porous bed, J. Heat Transfer 112 (1990) 690–699.

[8] A. Amiri, K. Vafai, Analysis of dispersion effects and non-thermal equilibrium non-Darcian variable properties incompressible flow through porous media, Int. J. Heat Mass Transfer 37 (1994) 939–954.

[9] A. Bejan, Convective Heat Transfer, second ed., Wiley, New York, 1995.

[10] T.J. Lu, C. Chen, Thermal transport and fire retardance properties of cellular aluminum alloys, Acta Mater. 47 (1999) 1469–1485.

[11] S. Torquato, L.V. Gibiansky, M.J. Silva, L.J. Gibson, Effective mechanical and transport properties of cellular solids, Int. J. Mech. Sci. 40 (1998) 71–82.

[12] Y. Asako, H. Nakamura, M. Faghri, Developing laminar flow and heat transfer in the entrance region of regular polygonal ducts, Int. J. Heat Mass Transfer 31 (1988) 2590–2593.

[13] H.E.M. Hunt, The mechanical strength of ceramic honeycomb monoliths as determined by simple experiments, Trans. Inst. Chem. Eng. A 71 (1993) 257–266.

[14] H.G. Allen, Analysis and Design of Structural Sandwich Panels, Pergamon Press, Oxford, 1969.

[15] B. Budiansky, On the minimum weights of compression structures, Int. J. Solids Struct. 36 (1999) 3677–3708.